Environmental Science and Pollution Research (2022) 29:19583–19593
https://doi.org/10.1007/s11356-021-17187-x

RESEARCH ARTICLE

Photocatalytic degradation of imidacloprid by optimized Bi_2WO_6/NH_2-MIL-88B(Fe) composite under visible light

Mao-Long Chen[1] · Tian-Hui Lu[1] · Shan-Shan Li[1] · Li Wen[1] · Zhou Xu[1] · Yun-Hui Cheng[1]

Received: 27 August 2021 / Accepted: 20 October 2021 / Published online: 31 October 2021

Abstract

Imidacloprid as a widely used neonicotinoid insecticide can cause harmful pesticide residue inevitably. Metal-organic frameworks (MOFs) were innovatively composited to improve the light absorption and degradation performance of Bi_2WO_6 semiconductor, which expanded the photodegradation application in solving environmental problems. Based on the synergistic effect of Bi_2WO_6 and NH_2-MIL-88B(Fe), a Bi_2WO_6/NH_2-MIL-88B(Fe) (BNM) heterojunction photocatalyst with high-performance of photocatalytic degradation activities was successfully synthesized. The optimized BNM catalyst had a good degradation rate under visible light, which was mainly caused by generation of the active ·OH. Transient photocurrent response and electrochemical impedance tests verified that 1:2 BNM exhibits a highest charge separation and a lowest carrier recombination rate which were favorable to the photocatalytic activity. Cycle experiments show that the composite photocatalyst had good reusability and stability which were very important for potential industry applications.

Keywords Degradation · Metal-organic frameworks · Bi_2WO_6 · Photocatalytic · Imidacloprid · Heterojunction

Introduction

Imidacloprid (IMC) is the most widely used pesticide as a neonicotinoid insecticide, and it is often used to protect economic crops such as vegetables, tea trees and fruit trees. However, residual pesticides may form harmful intermediate products under the influence of the environment, which will pose a threat to humans and the environment (Satiroff et al. 2020). Photocatalytic degradation was always effective to reduce the residue of IMC in food and the environment. The pioneering photocatalyst was TiO_2, which opened a door to convert solar energy into valuable chemical energy (Rahimi et al. 2016). Subsequently, ZnO, CeO_2, ZnS, CdS, g-C_3N_4, and other have emerged in various fields of photocatalysis. However, the shortcomings of the above semiconductor materials, such as their prone to photocorrosion, rapid recombination of electron-hole, and slow catalytic kinetics on the surface, hindered their applications in eliminating the environmental contamination caused by IMC. Therefore, new photocatalysts with high photocatalytic activity and photostability are urgently needed.

Among many metal oxide photocatalysts, Bi-based metal oxide with low toxicity and high reserves have been successfully developed in recent years, such as Bi_2O_3 (Zhang et al. 2014), Bi_2WO_6 (Fu et al. 2005, Karbasi et al. 2019, Karbasi et al. 2020), $BiVO_4$ (Kohtani et al. 2005), $Bi_4V_2O_{11}$ (Chen et al. 2013), $BiPO_4$ (Lv et al. 2014), $Bi_2O_2CO_3$ (Madhusudan et al. 2012), $BiFeO_3$ (Humayun et al. 2016), BiOX (Zhang et al. 2012) (X = Cl, Br, I), $BiNbO_4$ (Bakiro et al. 2020), and other semiconductors. As one of the simplest Aurivillius oxides, bismuth tungstate (Bi_2WO_6) has a suitable band gap, high photoactivity and stability, non-toxicity, and low cost, which has attracted many attentions (Dona-Rodriguez and Pulido Melian 2021). The perovskite crystals of Bi_2WO_6 have a layered structure, which facilitates the migration of the light carrier and thus enhances its photocatalytic performance. However, the pure Bi_2WO_6 material is also a low-efficiency semiconductor, owing to its poor visible light response, low e^--h^+ migration efficiency and high recombination efficiency; thus, many strategies have been adopted to

Responsible Editor: Sami Rtimi

✉ Mao-Long Chen
mlchen@xmu.edu.cn

✉ Yun-Hui Cheng
cyh@csust.edu.cn

[1] College of Chemistry and Food Engineering, Changsha University of Science & Technology, Changsha, Hunan, China

boost the photocatalytic performance of Bi_2WO_6 semiconductor materials, such as morphology modification, surface modification and other photocatalyst composites. Currently, Bi_2WO_6 is often combined with g-C_3N_4 (Al-Namshah and Mohamed 2021), CdS (Zhang et al. 2021), CuS (Mao et al. 2021), rGO (Zhao et al. 2021), and Co_3O_4 (Sun et al. 2021) to synthesize composite catalysts to improve catalytic performance. However, these composites still did not solve all the upper challenges, thus the metal-organic framework (MOF)-based photocatalysts come into our sight due to their high photocatalytic performance and good chemical stability (Mirhosseini et al. 2021).

In recent years, MOFs, as a kind of porous materials with applications in many areas (Chen et al. 2021b, Xu et al. 2021), also have been extensively studied in the treatment of small organic pollutants (Zhang et al. 2019). By combining the advantages of metal oxide semiconductors (MOS) and MOFs, MOS/MOF composites have become a kind of universal photocatalyst (Gautam et al. 2020). Moreover, due to the synergistic effect between the components, the MOS/MOFs composite photocatalysts usually show a higher catalytic activity than that of the alone material. Thus, few composite materials of Bi_2WO_6/MOFs (UiO-66, MIL-53, MIL-125 and MIL-100) photocatalysts were reported for the degradation of Rhodamine B (Sha et al. 2014, Tu et al. 2020, Xu et al. 2020) and tetracycline (He et al. 2021) recently. However, only four MOFs and only two degradation targets were investigated, more efforts are needed for this kind of photocatalyst.

Previously, we found out that NH_2-MIL-88B(Fe) was an effective adsorbent and Fenton-like catalyst for degradation of IMC by the active substance of ·OH (Chen et al. 2021a). Thus, NH_2-MIL-88B(Fe) was chosen to composite with Bi_2WO_6 to produce a photocatalyst with high performance. Herein, a serials of composite materials Bi_2WO_6/NH_2-MIL-88B(Fe) (BNM) heterojunction with different molar ratios were hydrothermally synthesized. The visible photodegradation performances of BNM heterojunction to IMC were studied. The introduction of NH_2-MIL-88B(Fe) may enhance the adsorption capacity, accelerate the transfer of e^--h^+, and even broaden the range of light absorption. In the present study, the relationship between the structure and the photocatalytic activity of the photocatalyst was investigated, and the free radical capture results verified that ·OH was the main active substances in this system.

Experimental section

Synthesis

NH_2-MIL-88B (Fe) was synthesized by hydrothermal method as reported (Chen et al. 2021a). Firstly, $FeCl_3·6H_2O$ (2.0 mmol, 0.54 g) and NH_2-BDC (2.0 mmol, 0.36 g) were added into DMF (42.0 mL), and then the mixture was stirred at room temperature for 10 min. Subsequently, the mixture was transferred to a 100 mL Teflon reactor and heated at 383 K for 12.0 h. After the reactor was cooled to room temperature, the suspension was centrifuged at a centrifugal force of 5000*g* for 5.0 min to obtain a brown product, which was washed 3 times with DMF and EtOH, respectively. Finally, the product was dried in a vacuum oven at 343 K for 12.0 h.

The preparation process of Bi_2WO_6/NH_2-MIL-88B(Fe) samples was as following reports with some modifications (Hu et al. 2019, Zhang et al. 2013). Disperse 1.0 mmol (0.33 g) of $Na_2WO_4·2H_2O$ and 0.5 mmol (0.16 g) of NH_2-MIL-88B(Fe) in 20.0 mL of ethylene glycol to form solution A. Then, the solution B formed by 2.0 mmol (0.97 g) $Bi(NO_3)_3·5H_2O$ and 25.0 mL of 2.0 mol/L HNO_3 was added drop-wisely to solution A. After mixing evenly, the pH of the suspension was adjusted to 4.0, and the suspension was stirred at room temperature for six hours. Then, the suspension was transferred to a 100 mL Teflon reactor and heated at 393 K for 12.0 h. The resulting powder was washed with distilled water and ethanol. Finally, after drying at 333 K for 12.0 h, the product Bi_2WO_6/NH_2-MIL-88B(Fe) (designated as 1:0.5-BNM) was obtained. By changing the molar amount of NH_2-MIL-88B(Fe) added, composite photocatalysts of 1:0.3 BNM, 1:0.5 BNM, 1:1 BNM, 1:2 BNM and 1:3 BNM can be synthesized respectively.

Characterization

The high-resolution thermal field emission scanning electron microscope was recorded by the Quanta 400 FEG instrument (FEI Company, USA). The X-ray powder diffraction patterns were recorded by a BRUKER AXS D8-Advance X-ray instrument, and the test conditions were the scanning range of 5°–45° and the scanning speed of 8°/min. Fourier infrared spectroscopy analysis were recorded by a Nicolet FT-IR 5700 spectrometer. The surface areas of the catalyst were measured by the American Mike TriStart II 3020 automatic multi-station specific surface area and porosity analyzer. Ultraviolet-visible diffuse reflectance spectroscopy was a full-wavelength scan performed by Shimadzu UV-3600 plus of Japan. The transient photocurrent response was based on the traditional three-electrode system, the electrolyte was 0.5M Na_2SO_4 solution, the time was 200 s, and the applied bias voltage was 0.7V vs. saturated silver/silver chloride electrode. The electrochemical impedance was measured by Shanghai Chenhua CHI-660C equipment, using a standard three-electrode device.

Photodegradation experiments

Before irradiating with visible light, perform the adsorption process in the dark. After a certain amount of photocatalyst was added into IMC solution (50.0 mL), the dark adsorption process lasts for 30.0 minutes. Then Zhongke Microenergy CME-Xe300F model xenon lamp (λ> 400 nm, China) was utilized to irradiate photocatalytic process. The catalyst was removed through a 0.22-μm syringe filter. A high performance liquid chromatography (Waters 2695, USA) was used to quantitatively detect the IMC at a wavelength of 270 nm (Chen et al. 2021a). The changes in concentrations were represented by C/C_0, where C_0 and C were the original concentration and residual concentration of IMC, respectively.

Results and discussion

Characterizations

The powder XRD patterns of composite photocatalysts such as pure NH_2-MIL-88B(Fe), pure Bi_2WO_6, and different molar ratio BNM are shown in the range of 5° < 2θ < 80° (2θ) in Fig. 1a. The diffraction peaks of pure Bi_2WO_6 at 28.3°, 32.8°, 47.1°, 55.9°, 58.6°, 68.8°, 76.1°, 78.4° can be attributed to the crystal faces (1 3 1), (2 0 0), (2 0 2), (3 3 1), (2 6 2), (0 8 3), (1 9 3), (2 0 4) of the orthorhombic phase (Bi_2WO_6, PDF#39-0256) (Zhao et al. 2018), indicating the high crystalline quality of Bi_2WO_6. The BNM composite photocatalysts with different molar ratios all showed different levels of characteristic absorption peaks of Bi_2WO_6 and NH_2-MIL-88B(Fe), which could verify the successful composites synthesis. In order to determine certain chemical vibration bands in the composite material, the FT-IR spectra of the pure Bi_2WO_6, NH_2-MIL-88B(Fe) and BNM composite photocatalyst with different molar ratio are shown in Fig. 1b. The absorption peaks of Bi_2WO_6 at 443 cm^{-1}, 587 cm^{-1}, and 817 cm^{-1} can be ascribed to the vibrations of the Bi–O bond, the absorption peak at 730 cm^{-1} can be attributed to the W–O bond (Zhang 2017), and the absorption band in the range of 3415-3435 cm^{-1} is related to the vibrations of O–H bond (Aljerf 2018). As the ratio of NH_2-MIL-88B(Fe) increases, its characteristic absorption peaks increase, indicating that NH_2-MIL-88B(Fe) has been successfully integrated into the BNM composite photocatalyst. SEM image shows the aggregated morphology of the obtained samples

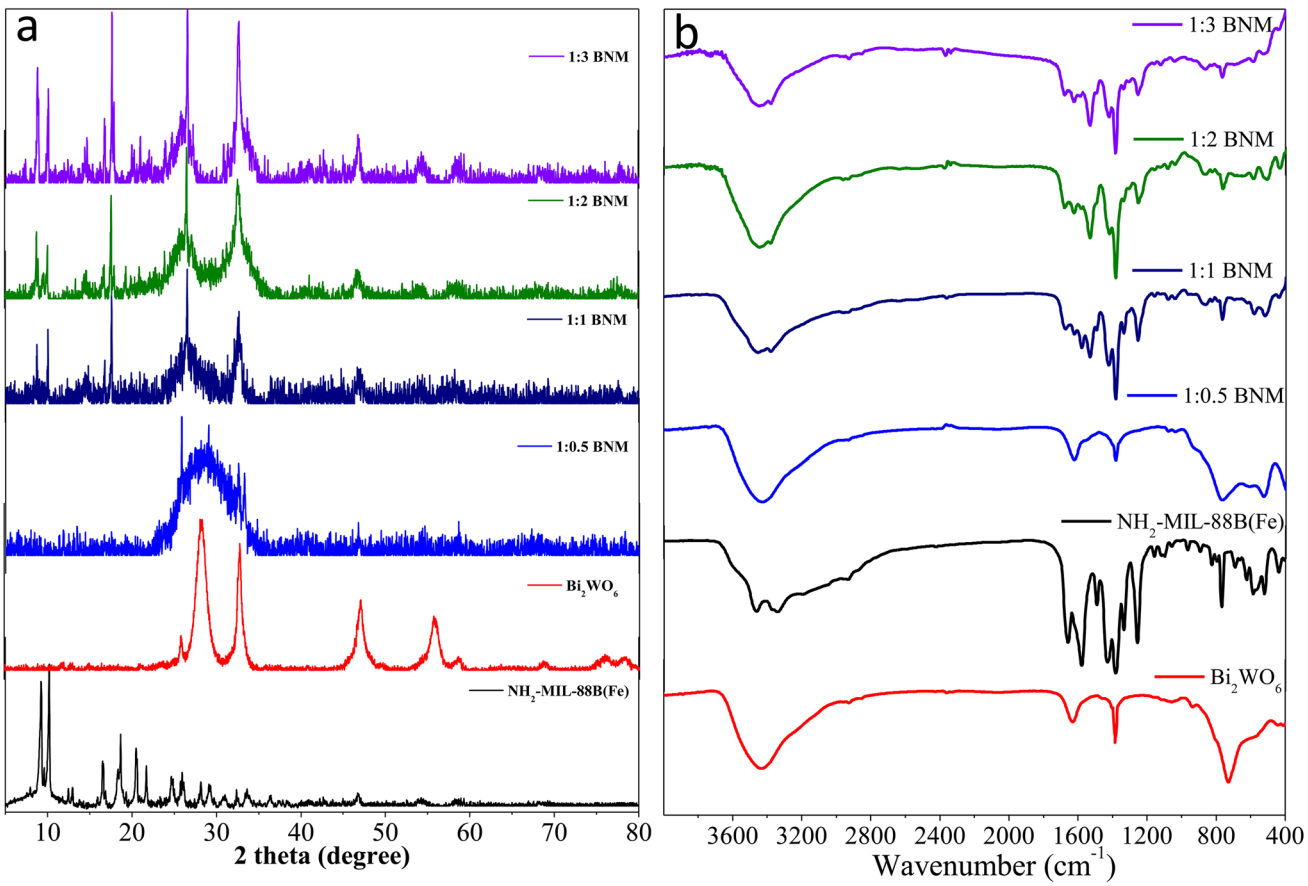

Fig. 1 **(a)** XRD patterns. **b** FT-IR spectra of as-prepared composite photocatalytic material

(Fig. S1, supporting information). Pure Bi_2WO_6 has several disordered nanosheets, and the 1:2 BNM composite exhibits a large volume morphology with many nanosheets. EDS and elemental diagrams showed that Bi_2WO_6 contained C, N, O, W and Bi elements, and C, N, O, W, Fe, and Bi elements were present in the 1:2 BNM complex.

X-ray photoelectron spectroscopy (XPS) analysis of NH_2-MIL-88B(Fe), Bi_2WO_6, and 1:2 BNM were carried out to study the surface chemical compositions of the photocatalyst. In the entire spectra of XPS (Fig. S2), Bi, W, Fe, and C elements can be observed in 1:2 BNM. The signal peak of C 1*s* may be caused by CO_2 in the air (Wan et al. 2017). In Fig. 2a–d, the high-resolution Bi 4*f* spectrum of Bi_2WO_6 semiconductor shows two peaks at 165.1 and 159.8 eV, corresponding to Bi $4f_{5/2}$ and Bi $4f_{7/2}$, respectively. The peaks at 38.3 and 36.1 eV can be ascribed to W $4f_{5/2}$ and W $4f_{7/2}$ respectively. The peak at 530.7 eV may correspond to O1*s*. The binding energy of 1:2 BNM Bi 4*f*, W 4*f* and O 1*s* is almost the same as that of pure Bi_2WO_6. In the Fe 2*p* spectrum, the Fe $2p_{1/2}$ and Fe $2p_{3/2}$ characteristic absorption peaks of 1:2 BNM are similar to those of NH_2-MIL-88B(Fe). The above characterization results indicate that the 1:2 BNM heterojunction is successfully synthesized.

The surface areas and corresponding pore size distributions of the pure Bi_2WO_6, NH_2-MIL-88B(Fe) and 1:2 BNM composite photocatalyst materials were analyzed by N_2 adsorption-desorption analysis method. As shown in Fig. 3, isotherms of all samples are type IV and showed obvious mesoporous characteristics with H3 type hysteresis loop, Bi_2WO_6 has the largest S_{BET} of 70.556 $m^2\ g^{-1}$ (Table 1), and 1:2 BNM material has a larger S_{BET} than that of NH_2-MIL-88B(Fe).

Catalytic degradation of IMC

Effect of different molar ratios of BNM

In order to screen out the photocatalyst with the best degradation effect, the visible photocatalytic activity to IMC of different catalysts were investigated. As shown in Fig. 4, IMC did not self-degrade under visible light, and all catalysts could promote the degradation of IMC, and the 1:2 BNM composite showed the best activity among them. As the mass of NH_2-MIL-88B (Fe) increases, the degradation efficiency first increases and then decreases. When the molar ratio of Bi_2WO_6 to NH_2-MIL-88B(Fe) was 1:3, most

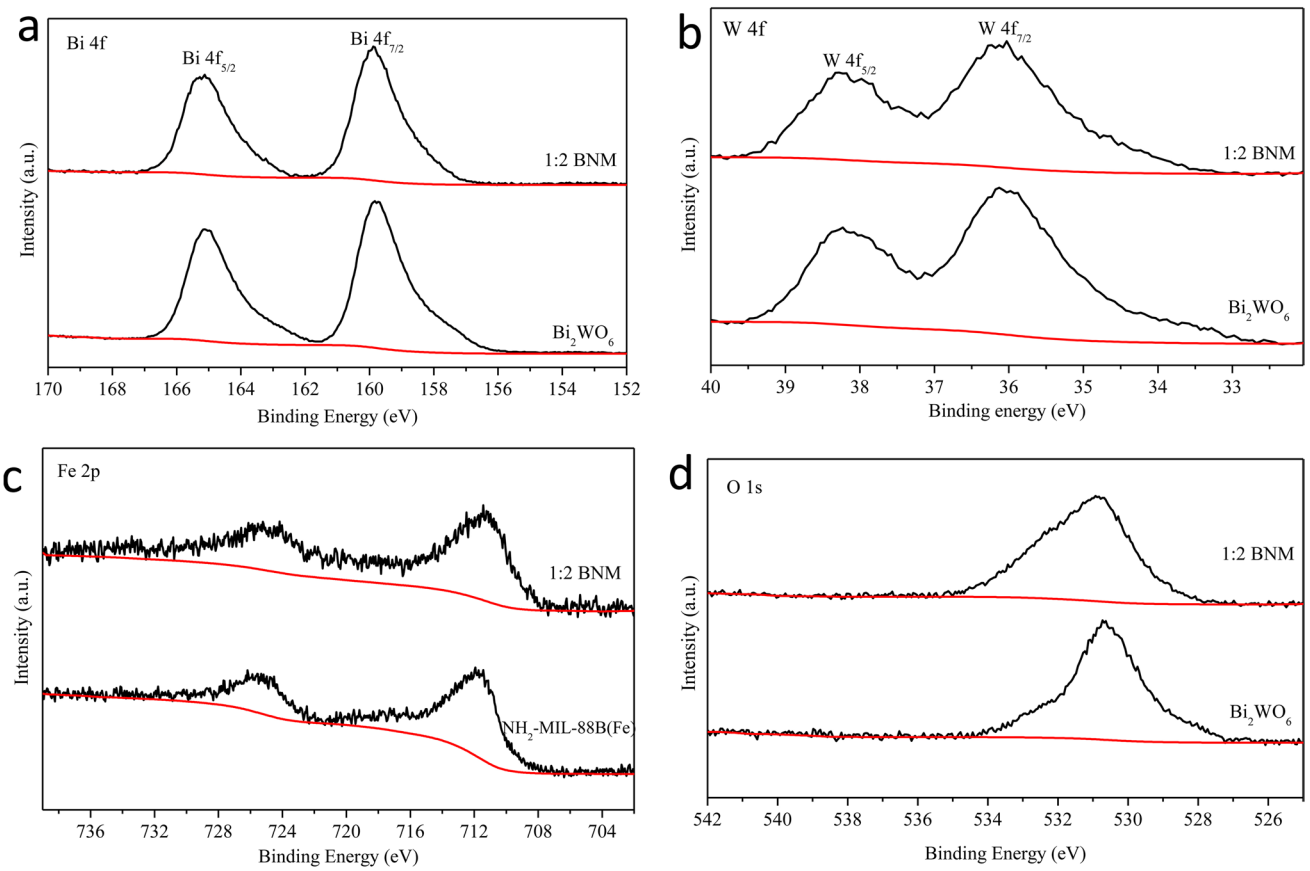

Fig. 2 XPS spectra of NH_2-MIL-88B(Fe), Bi_2WO_6 and 1:2 BNM: high-resolution spectra of Bi 4*f* (**a**), W 4*f* (**b**), Fe 2*p* (**c**), O 1*s* (**d**)

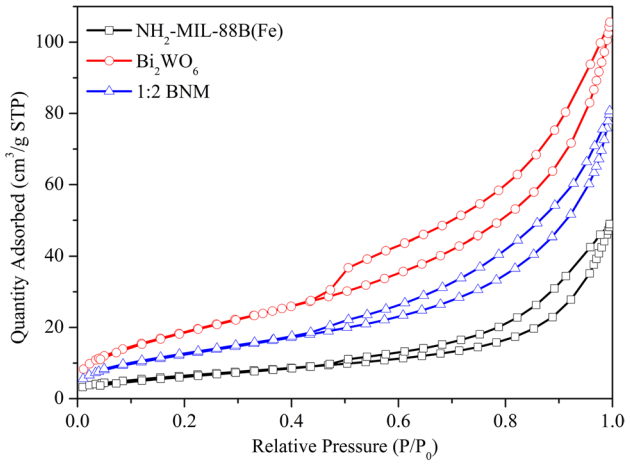

Fig. 3 Nitrogen adsorption–desorption isotherms of photocatalyst

Table 1 Parameters of S_{BET}, pore volume, and average pore size

Type of catalyst	S_{BET} ($m^2\ g^{-1}$)	Pore volume ($cm^3\ g^{-1}$)	Average pore size (nm)
NH_2-MIL-88B(Fe)	23.663	0.072520	11.1350
Bi_2WO_6	70.556	0.158530	8.0857
1:2 BNM	45.572	0.122179	9.40347

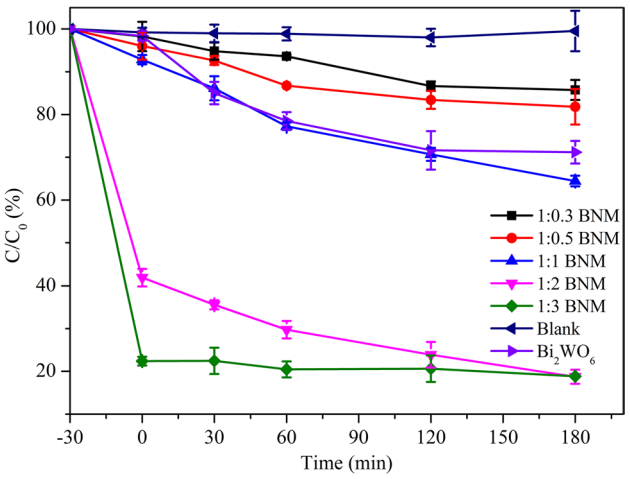

Fig. 4 Catalytic degradation of IMC by photocatalysts with different molar ratios (experimental conditions: 0.4 g/L material, 15 mg/L IMC)

of the IMC was adsorbed, and the photocatalytic ability was significantly inhibited. Therefore, 1:2 BNM was chose for subsequent experiments.

Effect of the reaction parameters

As shown in Fig. 5a, the effects of the initial concentrations of IMC (2–25 mg/L) on the degradation were investigated. The degradation ratio decreased with the increase of initial concentration. As the reaction concentration increases, Fig. 5b shows a linear relationship between -In(C/C_0) and the irradiation time *t*; thus, the first-order kinetic model could be applied to this system. The degradation rate constants *K* of 5.0, 10.0, 15.0, 20.0, and 25.0 mg/L IMC were 0.00479 min^{-1}, 0.00548 min^{-1}, 0.00321 min^{-1}, 0.00158 min^{-1}, and 0.00168 min^{-1}, respectively. Therefore, an initial concentration of 10.0 mg/L of IMC was chose for subsequent tests.

IMC (10.0 mg/L) was used to study the effect of the photocatalyst 1:2 BNM dose on the photocatalytic activity, and the results are shown in Fig. 5c. However, when the dosage increased to 0.50 g/L, the degradation ratio decreased. Excessive use of 1:2 BNM should be avoided, because the high concentration of the photocatalyst would lead to a decrease in light transmittance, which would cause a decrease of the degradation efficiency to IMC pollutants. Therefore, 0.40 g/L 1:2 BNM composite photocatalyst was selected in the follow-up experiment. Performing first-order kinetic fitting, where the 1:2 BNM degradation IMC fitting rate constants *k* of 0.1, 0.2, 0.3, 0.40, and 0.50 g/L were 0.00395 min^{-1}, 0.00207 min^{-1}, 0.00242 min^{-1}, 0.0054 min^{-1}, and 0.00124 min^{-1} (Fig. 5d), it is obvious that the degradation rate of 0.40 g/L 1:2 BNM was the fastest one.

The pH of the reaction system has a great influence on the adsorption and photocatalytic reactions. Here, we adjusted the pH value of the initial IMC solution by using 1.0 M HCl or NaOH solution. The effects of pH of the initial solution from 3.0 to 11.0 on the photocatalytic degradation of IMC were studied (Fig. 5e). The fitting rate constants k were 0.00196 min^{-1}, 0.00337 min^{-1}, 0.00471 min^{-1}, 0.00425 min^{-1}, 0.0054 min^{-1}, and 0.00185 min^{-1} (Fig. 5f). Obviously, when pH value was 9.0, this system had the fastest degradation rate.

Evaluation of photocatalytic properties

The UV-Vis DRS absorption spectra of the sample are shown in Fig. 6a. It can be clearly observed that compared with pure Bi_2WO_6, the light absorption range of composite 1:2 BNM is further expanded to the visible light region. However, the light absorption capacity of NH_2-MIL-88B(Fe) is similar to that of 1:2 BNM, which is not sufficient to show that the BNM heterojunction significantly improves the photocatalytic activity.

The conversion characteristic curve of the photocatalyst is used to detect whether the catalyst is sensitive to light. As can be seen from the Fig. 6b, in the traditional three-electrode system with the electrolyte of 0.50 M Na_2SO_4

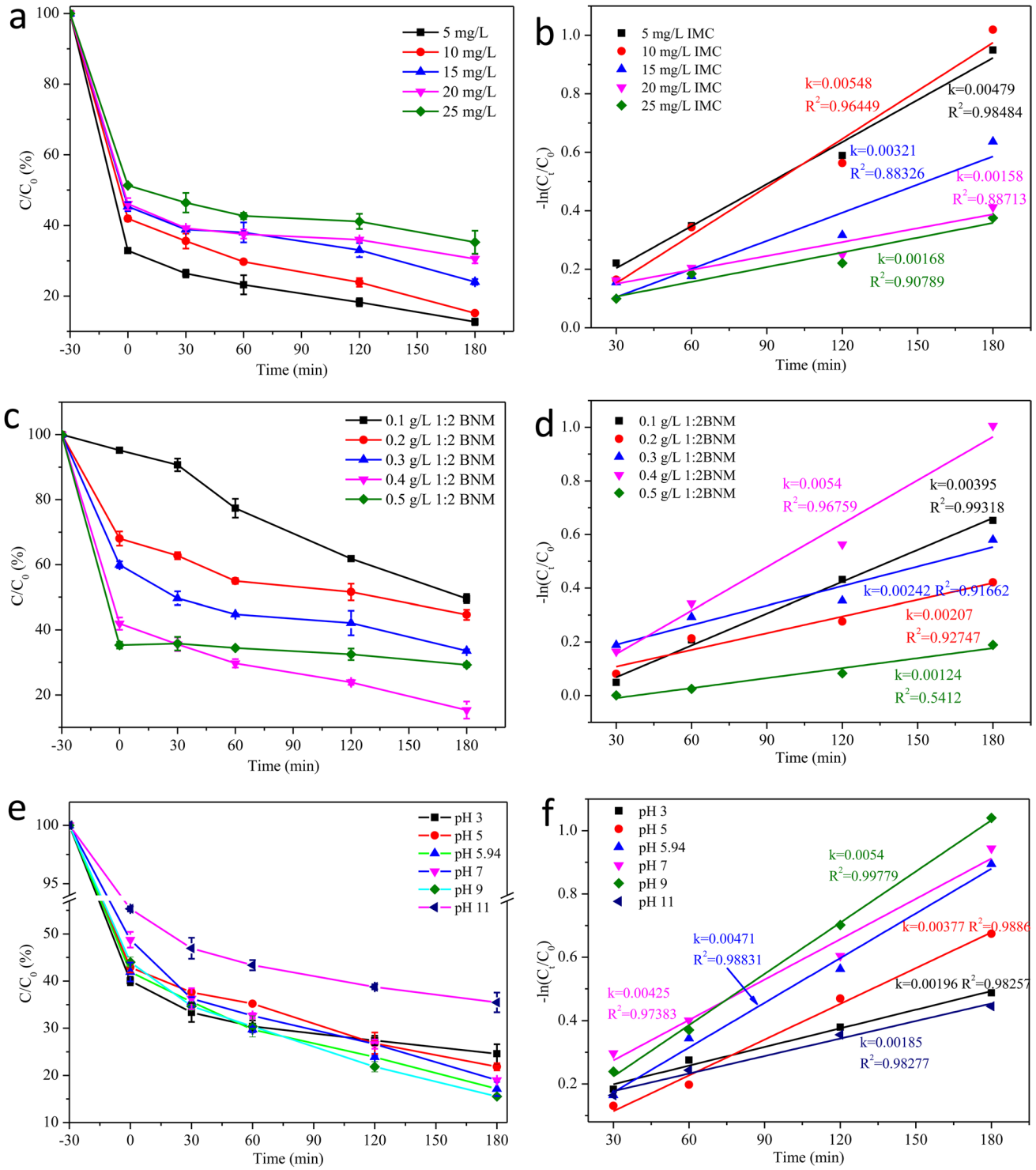

Fig. 5 **(a)** IMC concentration. **b** IMC concentration rate diagram. **c** Photocatalyst concentration. **d** Photocatalyst rate diagram. **e** Initial pH. **f** Initial pH rate diagram

aqueous solution, the current of 1:2 BNM catalyst is very low in the dark state, but the current rises quickly when turning on the light. It can be seen that the catalyst is very sensitive to light, and the photosensitivity of the sample will not be reduced when the catalyst is switched on and off repeatedly.

Electrochemical impedance spectroscopy (EIS) measurement is used to study the properties of catalyst charge

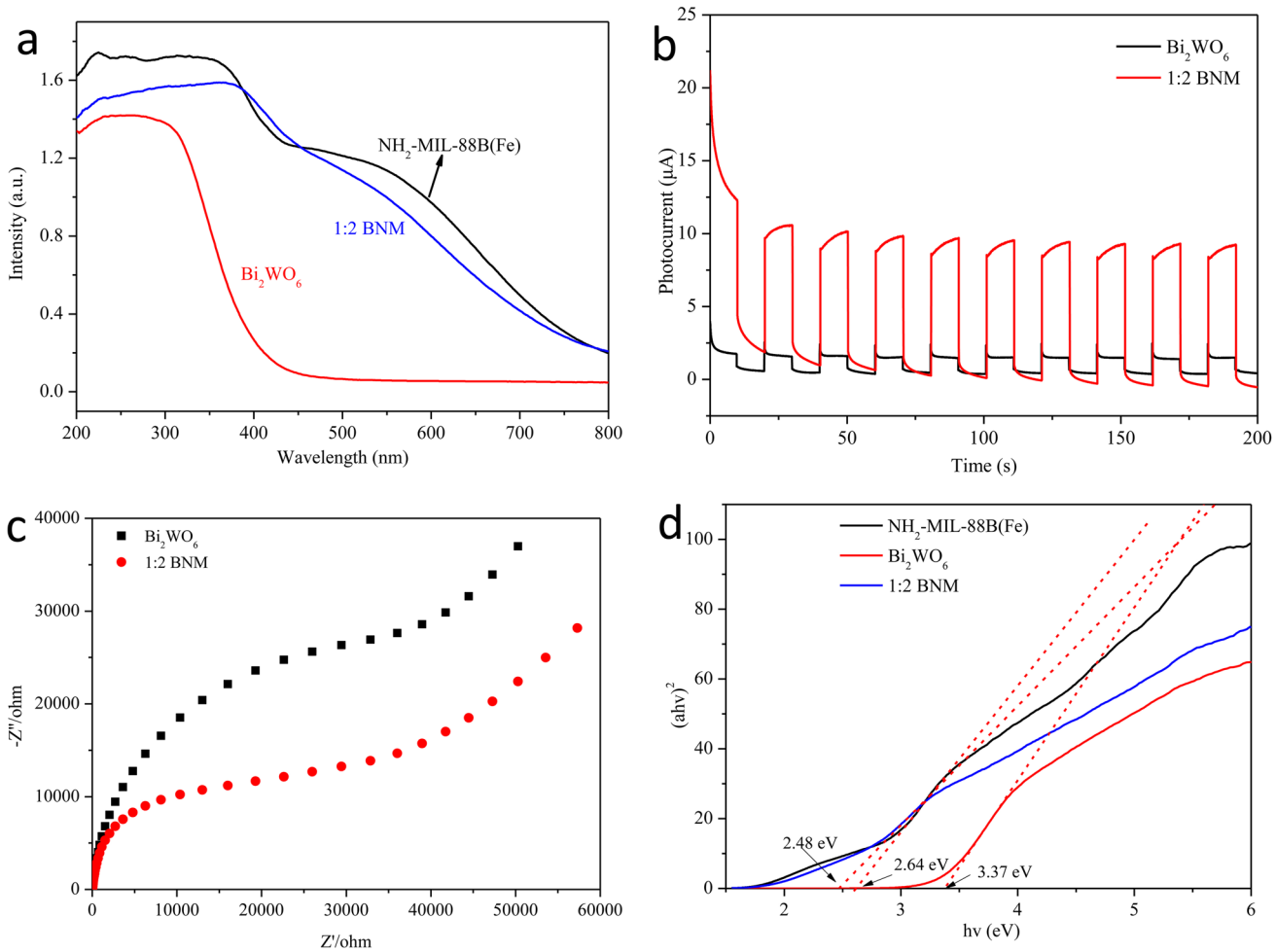

Fig. 6 **(a)** UV–vis DRS absorption spectra. **b** Transient photocurrent spectra and **c** EIS spectra of the as-obtained samples under the irradiation of visible light; (d) plots of $(\alpha h\nu)^2$ vs photon energy of as-prepared samples

transfer and recombination. The arc diameter represents the charge transfer resistance (R_{ct}). The smaller the arc diameter, the lower the R_{ct}. Figure 6c shows that 1:2 BNM has more effective photogenerated electron-hole separation and faster interface charge transfer than Bi_2WO_6. According to the above results, it can be concluded that the combination of NH_2-MIL-88B(Fe) and Bi_2WO_6 is an effective method to promote the photocatalytic efficiency. The main reason for the enhanced activity of 1:2 BNM is the effective charge separation and transfer ability.

In Fig. 6d, based on the Kubelke–Munk transformation, the band gaps (Eg) of NH_2-MIL-88B (Fe) and Bi_2WO_6 are 2.64 and 3.37 eV, respectively. In addition, the conduction band potential and valence band potential can be calculated according to Eqs. (1) and (2), where the χ values of Bi_2WO_6 and NH_2-MIL-88B (Fe) are 6.36 (Ju et al. 2014) and 5.86 (Na et al. 2018), respectively. Then, the potentials of the conduction band (CB) are calculated to be 0.04 eV and 0.175 eV/NHE for NH_2-MIL-88B (Fe) and Bi_2WO_6, respectively. The potentials of valence band (VB) are 2.680 eV and 3.545 eV/NHE for NH_2-MIL-88B (Fe) and Bi_2WO_6, respectively. All in all, as shown in Table 2, this catalyst shows an acceptable degradation ratio with low-level catalyst dosage. Although the catalyst of PANI/ZnO-$CoMoO_4$ shown the highest degradation ratio, the catalyst dosage was high for low concentration of IMC (163.5 mg for 4.5 mg/L in 4.0 mL) (Adabavazeh et al. 2021).

$$E_{CB} = \chi - E^c - 1/2E_g \quad (1)$$

$$E_{VB} = E_g + E_{CB} \quad (2)$$

where E_{VB} is the edge potential of VB, E_{CB} is the edge potential of CB, χ is the electronegativity, Eg is the band gap, E^C is the energy of free electrons on the hydrogen scale (about 4.5 eV).

Table 2 Comparison of photocatalytic activity of various photocatalysts to imidacloprid

Photocatalyst	Catalyst (mg)	IMC (mg/L)	pH	Solution (mL)	Time (h)	Degradation ratio (%)	Light type	Ref.
BiCo-MCP	***100***	10	1~3.5	100	5	75.8	Xenon lamp 300 W	(Liang et al. 2021)
PANI/ZnO-$CoMoO_4$	***163.5***	4.5	4	***4***	3	97	LED lamp 60 W	(Adabavazeh et al. 2021)
Ag_2O/g-C_3N_4	***100***	10	\	100	2	80	Xenon lamp 300 W	(Liang et al. 2019)
Ag-ZnO	40	20	10	100	1.3	***70***	UV tubes 18 W	(Kanwal et al. 2018)
Bi_2WO_6/NH_2-MIL-88B(Fe)	20	10	9	50	3	84	Xenon lamp 300 W	This work

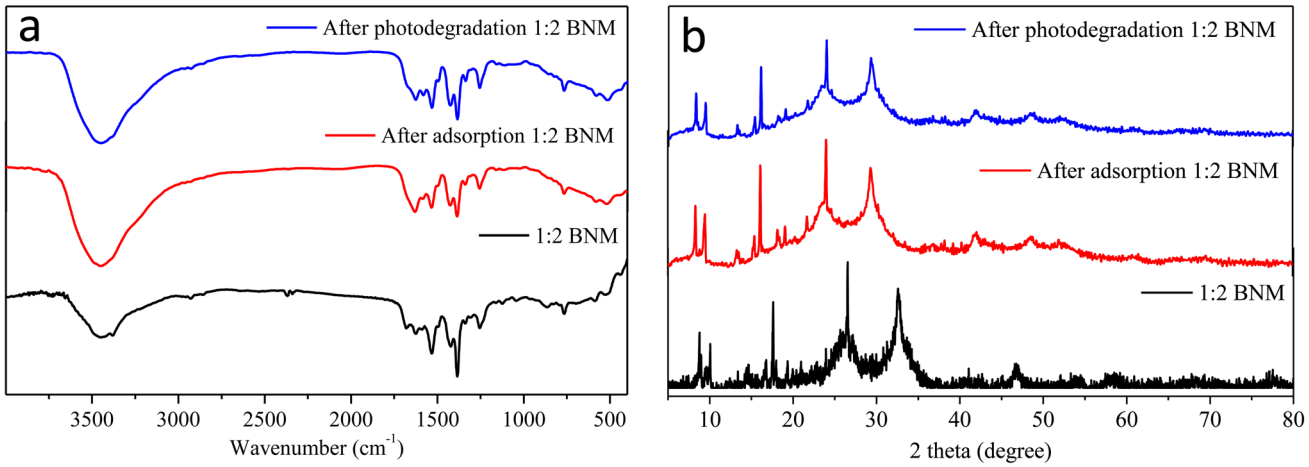

Fig. 7 (**a**) FT-IR and **b** XRD diagram of 1:2 BNM before and after reaction

Stability and reusability of BNM

The structure of 1:2 BNM before and after IMC degradation was characterized to evaluate the stability of the catalyst under the current experimental conditions. As can be seen from Fig. 7, the FT-IR and XRD spectra of 1:2 BNM before and after IMC adsorption and degradation did not change significantly. In addition, the stability and reusability of the composite material were further studied by conducting 5 cycles of dye degradation tests on 1:2 BNM. As shown in Fig. 8, as the number of cycles increases, the activity of the photocatalyst decreases slightly. The possible reason is that some IMC molecules and degradation products may be adsorbed in the pores of the composite material. These trapped molecules will reduce the accessible surface area of the catalyst, leading to a decrease in its activity. After 5 cycles, the stability of the 1:2 BNM photocatalyst did not decrease significantly, indicating that it has good stability.

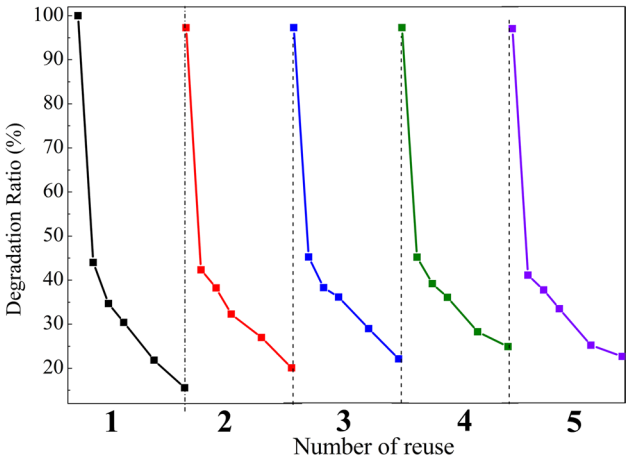

Fig. 8 Five-time reusable performance of composite photocatalyst 1:2 BNM

Possible mechanism of IMC degradation

Detection of active species

As shown in Fig. 9, IPA, BQ, and EDTA were used to capture ·OH, O_2^-, and h^+, respectively. Obviously, it can be seen that IPA and EDTA have significant inhibitory effects on the photocatalytic degradation ratio of 1:2 BNM, indicating that ·OH and h^+ are the main active substances. A LC-MS instrument was used to investigate the products of imidacloprid degradation as in previous report (Chen et al. 2021a). Owing to the products were similar to that of previous report, no detail results will be shown in here.

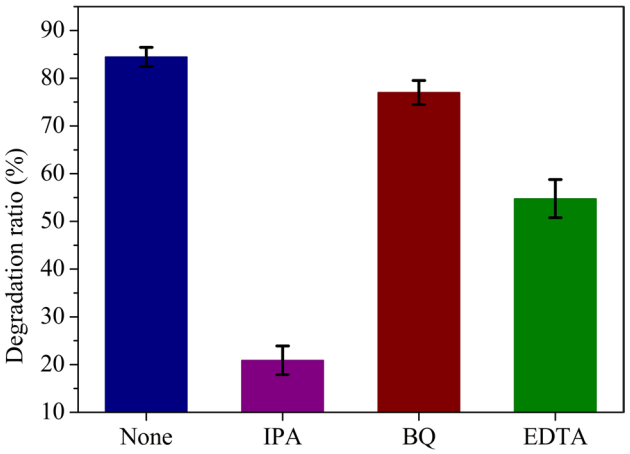

Fig. 9 Free radical capture experiment in the process of simulating 1:2 BNM degradation of IMC under sunlight

Possible photocatalytic mechanism

Based on the above results of active species, a possible photocatalytic degradation mechanism of IMC was proposed. As shown in Fig. 10, when the Bi_2WO_6 semiconductor and NH_2-MIL-88B(Fe) are irradiated by visible light, VB electrons can be excited by light to generate e^--h^+, and then the electron transition from VB to the CB happen and leave a corresponding number of h^+ in the VB. As the CB potential of NH_2-MIL-88B(Fe) is lower than that of Bi_2WO_6 (0.175 eV), the electron in CB of NH_2-MIL-88B(Fe) is easily transferred to CB of Bi_2WO_6. And the VB potential of Bi_2WO_6 (3.545 eV) is higher than that of NH_2-MIL-88B(Fe) (2.68 eV), which help the h^+ in VB of Bi_2WO_6 can easily transfer to VB of NH_2-MIL-88B(Fe). Thus, e^- aggregates in CB of Bi_2WO_6, while h^+ aggregates in VB of NH_2-MIL-88B(Fe), and achieving the charge separation. The VB potential of NH_2-MIL-88B(Fe) (2.68 eV) is higher than that of OH^-/·OH (2.38 eV), thus OH^- can generate ·OH easily under visible light. However, the CB potential of Bi_2WO_6 (0.1875 eV) is higher than the reduction potential of O_2/O_2^- (− 0.33 eV vs. NHE), thus it is difficult to generate $\bullet O_2^-$ from O_2 under visible light. This is also consistent with the free radical quenching experiment, so based on the analysis, a reasonable photocatalytic mechanism of this composite catalyst was proposed, which is similar but not same to the reported results (He et al. 2021, Tu et al. 2020).

Conclusion

In summary, a hydrothermal method was developed to prepare Bi_2WO_6/NH_2-MIL-88B(Fe) heterostructures. The prepared composite material exhibits better adsorption affinity and photocatalytic activity than that of Bi_2WO_6 for the

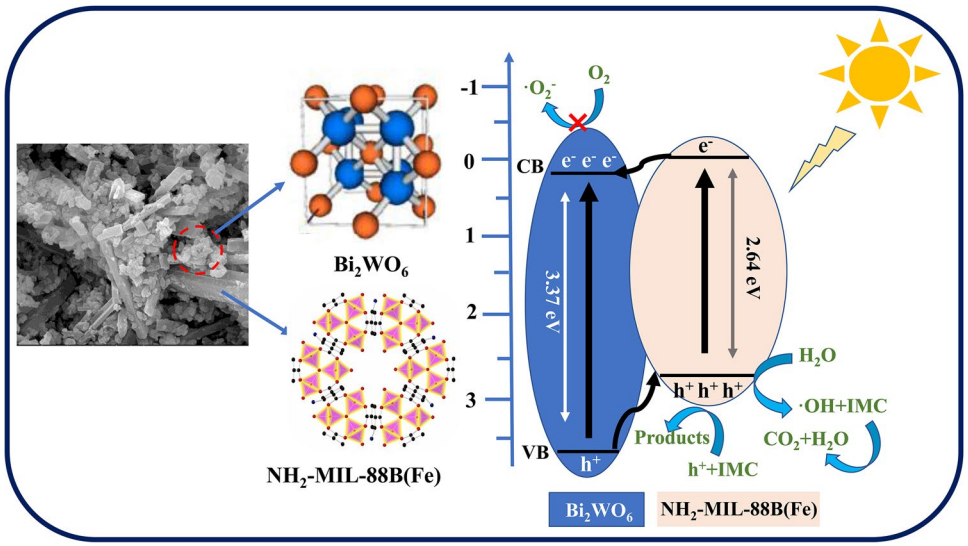

Fig. 10 Possible schematic diagram of the photocatalytic mechanism of 1:2 BNM composite photocatalyst

photodegradation to IMC under visible light. 1:2 BNM (the best molar ratio Bi_2WO_6: NH_2-MIL-88B(Fe)) can remove 84.46% of IMC through co-adsorption and visible light-induced photocatalytic degradation. This is mainly because NH_2-MIL-88B (Fe) can enhance charge transfer and inhibit electron-hole recombination effectively. Importantly, the cycle experiment also shows that the Bi_2WO_6/NH_2-MIL-88B(Fe) photocatalyst has good chemical stability and reusability which are necessary for the industrial applications.

Supplementary Information The online version contains supplementary material available at https://doi.org/10.1007/s11356-021-17187-x.

Author contribution MLC: conceptualization, validation, writing review and editing. THL: conceptualization, data curation, formal analysis, investigation, writing-original draft. SSL: conceptualization, data curation, formal analysis, investigation. LW: conceptualization, data curation, writing-review and editing. ZX: conceptualization, validation, writing-review and editing. YHC: resources, writing-review and editing.

Funding This research was funded by the National Natural Science Foundation of China (31601550) and Natural Science Foundation of Hunan (2019JJ50638).

Data availability The datasets used and/or analyzed during the current study are available from the corresponding author on reasonable request.

Declarations

Ethical approval Not applicable in this work.

Consent to participate Not applicable.

Consent to publish All authors read and approved the final manuscript.

Conflict of interest The authors declare no competing interests.

References

Adabavazeh H, Saljooqi A, Shamspur T, Mostafavi A (2021) Synthesis of polyaniline decorated with ZnO and $CoMoO_4$ nanoparticles for enhanced photocatalytic degradation of imidacloprid pesticide under visible light. Polyhedron 198. https://doi.org/10.1016/J.Poly.2021.115058

Al-Namshah KS, Mohamed RM (2021) Development of mesoporous Bi_2WO_6/g-C_3N_4 heterojunctions via soft- and hard-template-assisted procedures for accelerated and reinforced photocatalytic reduction of mercuric cations under vis light irradiation. Ceram Int 47:5003–5012. https://doi.org/10.1016/j.ceramint.2020.10.076

Aljerf L (2018) High-efficiency extraction of bromocresol purple dye and heavy metals as chromium from industrial effluent by adsorption onto a modified surface of zeolite: kinetics and equilibrium study. J Environ Manage 225:120–132. https://doi.org/10.1016/j.jenvman.2018.07.048

Bakiro M, Ahmed SH, Alzamly A (2020) Cycloaddition of CO_2 to propylene oxide using $BiNbO_4$/NH_2-MIL-125(Ti) composites as visible-light photocatalysts. J Environ Chem Eng 8:104461. https://doi.org/10.1016/J.Jece.2020.104461

Chen M-L, Lu T-H, Long L-L, Xu Z, Ding L, Cheng Y-H (2021) NH2-Fe-MILs for effective adsorption and Fenton-like degradation of imidacloprid: Removal performance and mechanism investigation. Environ Eng Res 27:200702. https://doi.org/10.4491/eer.2020.702

Chen ML, Ning P, Jiao Y, Xu Z, Cheng YH (2021) Extraction of antioxidant peptides from rice dreg protein hydrolysate via an angling method. Food Chem 337:128069. https://doi.org/10.1016/j.foodchem.2020.128069

Chen XF, Liu JB, Wang H, Ding YL, Sun YX, Yan H (2013) One-step approach to novel $Bi_4V_2O_{11}$ hierarchical hollow microspheres with high visible-light-driven photocatalytic activities. J Mater Chem A 1:877–883. https://doi.org/10.1039/c2ta00312k

Dona-Rodriguez JM, Pulido Melian E (2021) Nano-photocatalytic materials: possibilities and challenges. Nanomaterials-Basel 11 https://doi.org/10.3390/nano11030688

Fu H, Pan C, Yao W, Zhu Y (2005) Visible-light-induced degradation of rhodamine B by nanosized Bi_2WO_6. J Phys Chem B 109:22432–22439. https://doi.org/10.1021/jp052995j

Gautam S, Agrawal H, Thakur M, Akbari A, Sharda H, Kaur R, Amini M (2020) Metal oxides and metal organic frameworks for the photocatalytic degradation: a review. J Environ Chem Eng 8. https://doi.org/10.1016/J.Jece.2020.103726

He Y, Wang D, Li X, Fu Q, Yin L, Yang Q, Chen H (2021) Photocatalytic degradation of tetracycline by metal-organic frameworks modified with Bi_2WO_6 nanosheet under direct sunlight. Chemosphere 284:131386. https://doi.org/10.1016/j.chemosphere.2021.131386

Hu LX, Zhang YY, Lu WC, Lu YS, Hu HM (2019) Easily recyclable photocatalyst Bi_2WO_6/MOF/PVDF composite film for efficient degradation of aqueous refractory organic pollutants under visible-light irradiation. J Mater Sci 54:6238–6257. https://doi.org/10.1007/s10853-018-03302-w

Humayun M, Zada A, Li ZJ, Xie MZ, Zhang XL, Qu Y, Raziq F, Jing LQ (2016) Enhanced visible-light activities of porous $BiFeO_3$ by coupling with nanocrystalline TiO_2 and mechanism. Appl Catal B-Environ 180:219–226. https://doi.org/10.1016/j.apcatb.2015.06.035

Ju P, Wang P, Li B, Fan H, Ai SY, Zhang D, Wang Y (2014) A novel calcined Bi_2WO_6/$BiVO_4$ heterojunction photocatalyst with highly enhanced photocatalytic activity. Chem Eng J 236:430–437. https://doi.org/10.1016/j.cej.2013.10.001

Kanwal M, Tariq SR, Chotana GA (2018) Photocatalytic degradation of imidacloprid by Ag-ZnO composite. Environ Sci Pollut Res Int 25:27307–27320. https://doi.org/10.1007/s11356-018-2693-8

Karbasi M, Karimzadeh F, Kiwi J, Raeissi K, Pulgarin C, Rtimi S (2019) Flower-like magnetized photocatalysts accelerating an emerging pollutant removal under indoor visible light and related phenomena. J Photochem Photobio A: Chem 378:105–113. https://doi.org/10.1016/j.jphotochem.2019.04.017

Karbasi M, Karimzadeh F, Raeissi K, Rtimi S, Kiwi J, Giannakis S, Pulgarin C (2020) Insights into the photocatalytic bacterial inactivation by flower-like Bi_2WO_6 under solar or visible light, Through in situ monitoring and determination of reactive oxygen species (ROS). Water 12:1099

Kohtani S, Hiro J, Yamamoto N, Kudo A, Tokumura K, Nakagaki R (2005) Adsorptive and photocatalytic properties of Ag-loaded $BiVO_4$ on the degradation of 4-n-alkylphenols under visible light irradiation. Catal Commun 6:185–189. https://doi.org/10.1016/j.catcom.2004.12.006

Liang F, Lu M, Zhang YH, Shi Q, Shi FN (2021) Synthesis and structure of a bismuth-cobalt bimetal coordination polymer for green efficient photocatalytic degradation of organic wastes under visible light. J Mol Struct 1230. https://doi.org/10.1016/j.molstruc.2020.129636

Liang SH, Zhang DF, Pu XP, Yao XT, Han RT, Yin J, Ren XZ (2019) A novel Ag_2O/g-C_3N_4 p-n heterojunction photocatalysts with enhanced visible and near-infrared light activity. Sep Purif Technol 210:786–797. https://doi.org/10.1016/j.seppur.2018.09.008

Lv YH, Liu YF, Zhu YY, Zhu YF (2014) Surface oxygen vacancy induced photocatalytic performance enhancement of a $BiPO_4$ nanorod. J Mater Chem A 2:1174–1182. https://doi.org/10.1039/c3ta13841k

Madhusudan P, Yu J, Wang W, Cheng B, Liu G (2012) Facile synthesis of novel hierarchical graphene-$Bi_2O_2CO_3$ composites with enhanced photocatalytic performance under visible light. Dalton Trans 41:14345–14353. https://doi.org/10.1039/c2dt31528a

Mao W, Zhang LX, Wang TY, Bai YC, Guan YT (2021) Fabrication of highly efficient Bi_2WO_6/CuS composite for visible-light photocatalytic removal of organic pollutants and Cr(VI) from wastewater. Front Env Sci Eng 15:52. https://doi.org/10.1007/s11783-020-1344-8

Mirhosseini H, Shamspur T, Mostafavi A, Sargazi G (2021) A novel ultrasonic reverse micelle-assisted electrospun efficient route for Eu-MOF and Eu-MOF/CA composite nanofibers: a high performance photocatalytic treatment for removal of BG pollutant. Environ Sci Pollut Res Int 28:4317–4328. https://doi.org/10.1007/s11356-020-10746-8

Na Y, Miao S, Zhou L, Wei P, Cao Y (2018) Bio-inspired model of photosystem II: supramolecular assembly of an electron mediator into an SnO2 photoanode co-sensitized by a porphyrin photosensitizer and ruthenium molecular catalyst. Sustainable Energy Fuels 2:545–548. https://doi.org/10.1039/c7se00515f

Rahimi N, Pax RA, Gray EM (2016) Review of functional titanium oxides. I: TiO_2 and its modifications. Prog Solid State Chem 44:86–105. https://doi.org/10.1016/j.progsolidstchem.2016.07.002

Satiroff JA, Messer TL, Mittelstet AR, Snow DD (2020) Pesticide occurrence and persistence entering recreational lakes in watersheds of varying land uses. Environ Pollut 273:116399. https://doi.org/10.1016/j.envpol.2020.116399

Sha Z, Sun JL, Chan HSO, Jaenicke S, Wu JS (2014) Bismuth tungstate incorporated zirconium metalorganic framework composite with enhanced visible- light photocatalytic performance. Rsc Adv 4:64977–64984. https://doi.org/10.1039/c4ra13000f

Sun J, Shen CH, Guo J, Guo H, Yin YF, Xu XJ, Fei ZH, Liu ZT, Wen XJ (2021) Highly efficient activation of peroxymonosulfate by Co_3O_4/Bi_2WO_6 p-n heterojunction composites for the degradation of ciprofloxacin under visible light irradiation. J Colloid Interface Sci 588:19–30. https://doi.org/10.1016/j.jcis.2020.12.043

Tu Y, Ling LQ, Li QW, Long XY, Liu N, Li ZQ (2020) Greatly enhanced photocatalytic activity over Bi_2WO_6 by MIL-53 (Fe) modification. Opt Mater 110. https://doi.org/10.1016/J.Optmat.2020.110500

Wan SP, Zhong Q, Ou M, Zhang SL (2017) Synthesis and characterization of direct Z-scheme Bi_2MoO_6/$ZnIn_2S_4$ composite photocatalyst with enhanced photocatalytic oxidation of NO under visible light. J Mater Sci 52:11453–11466. https://doi.org/10.1007/s10853-017-1283-3

Xu YF, Zhou Y, Deng YH, Xiang Y, Tan YW, Tang HQ, Zou H (2020) Synthesis of Bi_2WO_6@NH_2-MIL-125(Ti): A S-Scheme Photocatalyst with Enhanced Visible Light Catalytic Activity. Catal Lett 150:3470–3480. https://doi.org/10.1007/s10562-020-03258-0

Xu Z, Long LL, Chen YQ, Chen ML, Cheng YH (2021) A nanozyme-linked immunosorbent assay based on metal-organic frameworks (MOFs) for sensitive detection of aflatoxin B1. Food Chem 338:128039. https://doi.org/10.1016/j.foodchem.2020.128039

Zhang JF, Hu YF, Jiang XL, Chen SF, Meng SG, Fu XL (2014) Design of a direct Z-scheme photocatalyst: Preparation and characterization of Bi_2O_3/g-C_3N_4 with high visible light activity. J Hazard Mater 280:713–722. https://doi.org/10.1016/j.jhazmat.2014.08.055

Zhang K, Liang J, Wang S, Liu J, Ren KX, Zheng X, Luo H, Peng YJ, Zou X, Bo X, Li JH, Yu XB (2012) BiOCl sub-microcrystals induced by citric acid and their high photocatalytic activities. Cryst Growth Des 12:793–803. https://doi.org/10.1021/cg201112j

Zhang XJ (2017) Synthesis and photocatalytic activity of Bi_2WO_6 microspheres with hierarchical structure. Ferroelectrics 514:34–42. https://doi.org/10.1080/00150193.2017.1359042

Zhang YH, Zhang N, Tang ZR, Xu YJ (2013) Identification of Bi_2WO_6 as a highly selective visible-light photocatalyst toward oxidation of glycerol to dihydroxyacetone in water. Chem Sci 4:1820–1824. https://doi.org/10.1039/c3sc50285f

Zhang YY, Liu Q, Yang C, Wu SC, Cheng JH (2019) Magnetic aluminum-based metal organic framework as a novel magnetic adsorbent for the effective removal of minocycline from aqueous solutions. Environ Pollut 255:113226. https://doi.org/10.1016/j.envpol.2019.113226

Zhang ZQ, Lin YZ, Liu F (2021) Preparation and photoelectric properties of Bi_2WO_6-CdS hybrid nanocrystals. Colloid Surface A 611:125883. https://doi.org/10.1016/j.colsurfa.2020.125883

Zhao Y, Liang X, Hu X, Fan J (2021) rGO/Bi_2WO_6 composite as a highly efficient and stable visible-light photocatalyst for norfloxacin degradation in aqueous environment. J Colloid Interface Sci 589:336–346. https://doi.org/10.1016/j.jcis.2021.01.016

Zhao YY, Wang YB, Liu EZ, Fan J, Hu XY (2018) Bi_2WO_6 nanoflowers: An efficient visible light photocatalytic activity for ceftriaxone sodium degradation. Appl Surf Sci 436:854–864. https://doi.org/10.1016/j.apsusc.2017.12.064